

Effect of Plasma Focusing Shots on Structural and Optical Properties of $Zn_{0.9}Co_{0.1}O$ Thin Films

E. R. Shaaban ^{1*}, Gamal El-Kashef², F. Diab² and A. S. Ali¹.

¹Physics Department, Faculty of Science, Al-Azhar University, P.O. 71452, Assiut, Egypt.

²Plasma and Nuclear Fusion Department, Nuclear Research Center, Atomic Energy Authority, Egypt.

Received: 5 Sep. 2015, Revised: 22 Oct. 2015, Accepted: 24 Oct. 2015.

Published online: 1 Jan. 2016.

Abstract: A $Zn_{0.9}Co_{0.1}O$ nanoparticles was made by a homogeneous precipitation method. Thin films of the same thickness of $Zn_{0.9}Co_{0.1}O$ were deposited onto highly cleaned glass substrates by the thermal evaporation technique using modified source. Thin films of the same thickness have been exposed to plasma focusing with 0, 5, 10 and 15 shots. The structural characteristics of $Zn_{0.9}Co_{0.1}O$ films were examined by X-ray diffraction (XRD) and scan electron microscope (SEM) before and after plasma focusing shots. The microstructure parameters, crystallites size and lattice strain have been found to reduce with increasing the plasma focusing shots. The optical properties were studied from their reflectance and transmittance in the spectral region in terms of the Murmann's equation. The refractive index has found to decrease with increasing PF shots own to the reduction in film thickness. The energy gap has also found to decrease with increasing the plasma focusing shots.

Keywords: $Zn_{0.9}Co_{0.1}O$; thin film; XRD; SEM; Plasma focusing.

1 Introduction

Plasma Focus (PF) device was developed in the earlier 60s [1] and found to be a wealthy plasma source of multi-radiation. Plasma focus discharge produces the short-lived plasma that is of high temperature and high density by making use of the self-generated magnetic field through electromagnetic acceleration and compression [2].

Recently, the Mother type has been used, it has been widely studied because of its low cost, a simplicity of engineering, various radiation and small dimensions in comparison with other radiation sources [3]. During the last decade, a rising interest in developing of low energy Plasma Focuses has been observed. The high efficiency of radiation production and relatively low costs of such devices cause mainly this process. PF as the ionizing radiation source is also more acceptable from the ecological point of view in comparison with isotopes, fission reactors, and classical accelerators. These sorts of radiation are produced at the high-current discharge in a chamber filled with various gases at a pressure of a few Pa.

It utilizes relatively low voltage and becomes a source of hard radiation only within a short period of time of the discharge period when pulsed electrical energy converts into the energy of beams of fast particles. Plasma Focus (PF) devices, which can produce dense magnetized plasmas, are known for more than 40 years as a powerful pulsed sources of X-rays (soft and hard), neutrons, fast electrons, ions and plasma streams. Emission characteristics of the PF facilities based strongly on technical parameters of the devices applied and on their operational conditions, i.e. charging voltage and pressure in the vacuum chamber. A PF is a source of quite high brightness due to its very short pulsed character and small sizes of the plasma source of radiation and all the rest time it is safe and does not require special store and guarding. One of the most dynamic spheres of modern industry is nanotechnology. It embraces precision engineering as well as electronics, electromechanical systems (such as the development of lab-on-a-chip' devices), biochips and other tools for gene engineering, drug manufacturing and delivery, sensors,

*Corresponding author E-mail: esam_ramadan2008@yahoo.com

diagnostics and analytical devices, etc. In the present work, we depict this DPF, its first performances and possible applications in thin films for the first time.

In the present work dilute magnetic semiconductors (DMS) created by doping transition metal (TM) ions into non-magnetic semiconductors have attracted a great deal of interest [4]. ZnO doped Co is promising material because of high solubility and excellent ferromagnetic near room temperature. Now, we examined the effect of plasma focusing shots on structural and optical properties of $Zn_{0.9}Co_{0.1}O$ thin films.

2 Experimental

A homogeneous solution was prepared by dissolving zinc acetate $Zn(CH_3COO)_2 \cdot 2H_2O$ (0.1 M) and $Co(NO_3)_2$ in (100 ml) distilled water. The solution was stirred for 15 min. The precipitate was dried at $100^\circ C$ for 2 h to obtain the drying precursor. The precursor was calcinated at $400^\circ C$ (according to thermogravimetric analysis, TGA) for 4 h to get nanoparticles of $Zn_{0.9}Co_{0.1}O$. The thermal behavior of the precursor was analyzed by thermogravimetric analysis (TGA) (Shimadzu 50 with an accuracy of ± 0.1 K).

Thin films with the same thickness of $Zn_{0.9}Co_{0.1}O$ were deposited by thermal evaporation of $Zn_{0.9}Co_{0.1}O$ from a modified source. It is a resistivity heated quartz crucible containing $Zn_{0.9}Co_{0.1}O$ powder and wrapped in a tantalum sheet. This arrangement was found to facilitate the loading of $Zn_{0.9}Co_{0.1}O$ powder and increase the lifetime of the heater. A small wad of quartz fiber wool was placed in the neck of quartz crucible to prevent spattering of $Zn_{0.9}Co_{0.1}O$ during outgassing and evaporation. This modified source proved to produce the film of high quality. The glass substrates were fixed onto substrate holder inside the vacuum chamber at the distance of about 20 cm above the evaporation source of a conventional coating unit (Edward 306A) and a vacuum of about 10^{-6} Pa. The evaporation rate, as well as the film thickness was controlled using a quartz crystal FTM6 monitor. The deposition rate was maintained 10 \AA/s constant throughout the samples preparation. Such a low deposition rate produces a film with a composition very close to that of the bulk starting material. The structure of the prepared samples powder and thin films was examined by XRD analysis (Shimadzu X-ray diffractometry 6000, Japan with $CuK\alpha$ radiation with $\lambda = 0.15418 \text{ nm}$). The intensity data were collected by step scan modes a 2θ range between 10 and 70 with the step size 0.02° and step time of 0.6 s. Pure silicon $\approx Si$ 99.9999 % was used as internal standard. The surface morphology of nanoparticles phases of powder were observed by means of a scanning electron microscope SEM (JOEL XL) operating an accelerating voltage of 30 kV. The optical transmittance T and reflectance R of the deposited films were measured using a UV-VIS-NIR Shimadzu UV-2101 double-beam spectrophotometer. The transmittance spectra

in the wavelength range 400–2500nm were collected at normal incidence without a substrate in the reference beam, whereas the reflectance spectra were measured using a reflection attachment close to normal incidence ($\sim 5^\circ$). In our measurements of R and T, the effect of slit correction was eliminated by adjusting the spectrophotometer slit width to 6 mm, which is much less than the width of the interference peaks observed in the transparent region of the investigated samples. All the optical measurements were made at room temperature. The experimental setup of the present plasma focusing device is shown in fig. 1. The system is energized by a capacitor bank consists of four capacitor which are connected in parallel and has a total capacitance of $30.84 \mu f$ and charged up to 8 KV giving a peak discharge current up to 150 kA. To initiate the discharge through the electrodes, a high voltage trigger was located near the spark gap which is a vital element since it is responsible for starting the breakdown just before the shots.

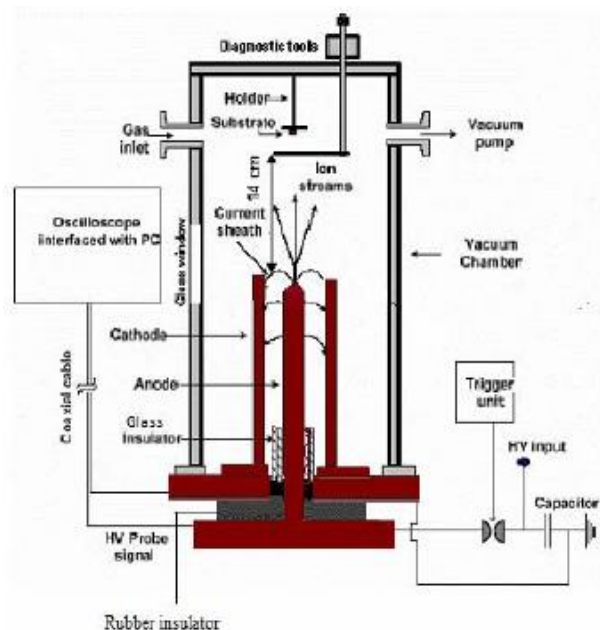


Fig.1 the schematic diagram of the PF device in Atomic Energy Authority, Egypt.

The cleaning process of the spark gap is carried out before and after 5 shots. The discharge chamber is made of stainless steel and has a length of 40 cm and diameter of 38 cm. Moreover, the electrodes of the plasma focus device in this experiment are a solid cylindrical tube to avoid the excessive hard x-ray emission from the anode surface due to electron bombardment. The plasma focus is operated with argon as the working gas. The device was evacuated to lower than 10^{-2} Pa before puffing Argon gas by rotary van pump) and filled with the required gas (argon) to a particular pressure (0.2–2 Pa) before the operation. This level of vacuum proved to be sufficient for operating with good focus in argon gas.

3. Results and discussion

3.1 Structural properties

In present work, the ion beams emitted from the plasma focusing (PF) devices have been employed by many researchers in plasma processing of materials including ion implantation, surface modification, thermal surface treatment, phase changes of thin film and thin film deposition [5-9]. The active species including ions and radicals assist the growth of films composed of nanoparticles with features quite different from those of the bulk substrate [10]. Subsequently, ion-surface interactions demand a careful consideration of various methods employed to evaluate the ion beam parameters in order to recognize the ion-induced surface changes. A much little is reported on the direct correlation of ion beam parameters with thin film properties including surface morphology, elemental composition and distribution, microstructure, microhardness and optical properties.

XRD pattern of $Zn_{0.9}Co_{0.1}O$ films deposited onto glass substrate is shown in Fig. 2.

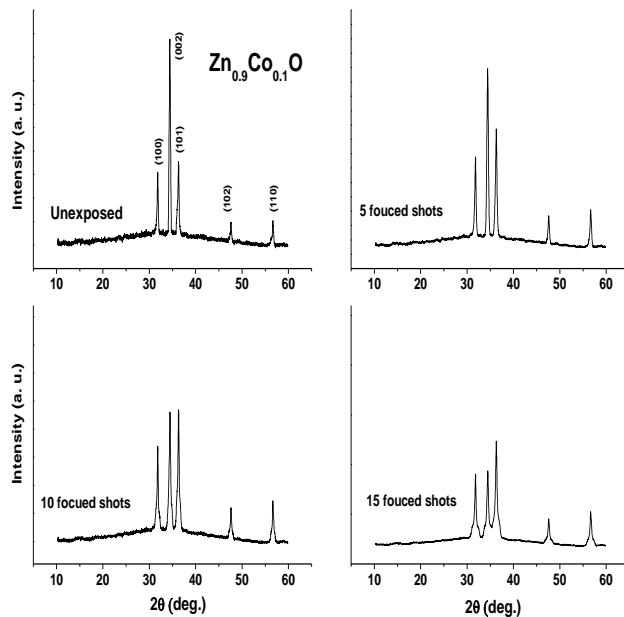


Fig. 2: XRD pattern of unexposed and exposed for 5, 10 and 15 plasma focusing shots of $Zn_{0.9}Co_{0.1}O$ thin films.

All of the diffraction peaks, which correspond to the planes (1 0 0), (0 0 2), (1 0 1), (1 0 2) and (1 0 0) are completely indexed to the hexagonal wurtzite ZnO structure (JCPDS 79-0205), revealing that the doping of Co does not change the crystal structure. The absence of individual metal (Co) or Co-related impurity phase diffraction peaks in the XRD spectra proves the formation of the $Zn_{0.9}Co_{0.1}O$ solid solution. The XRD spectra presented in Fig. 2 demonstrate the PF shots dependence of the ion-induced structural changes on the $Zn_{0.9}Co_{0.1}O$ thin

films exposed for 0, 5, 10 and 15 shots. The high energy of density of ion beams of very short (~140 nsec) pulse duration cause melting and subsequent rapid cooling of the thin film surface. Eventually, the original phases of the film

recrystallize with the development of a new phase during the molten state [11], which is more likely to occur due to the DPF ion induced stress effects. Fig. 2 shows a significant broadening of all the diffraction peaks of $Zn_{0.9}Co_{0.1}O$ thin films reveals the degradation of crystallinity of the substrate surface due to ion bombardment. An increase in the broadening of diffraction peaks with increasing in plasma focusing shots depicts the deposition of a $Zn_{0.9}Co_{0.1}O$ film with smaller grain sizes.

The microstructural parameters like grain size, crystal strain and dislocation density have been calculated. The average grain sizes (D) of $Zn_{0.9}Co_{0.1}O$ films were calculated from the XRD peaks using Scherrer's formula [12],

$$D_v = \frac{k'\lambda}{\beta \cos(\theta_o)} \quad (1)$$

Which D is the crystallite size, λ is the wavelength of the X-ray used, β is the full width at half maximum (FWHM) of diffraction peak in radians, θ is the corresponding Bragg angle and k' is a constant approximately equal 0.9. The lattice strain, ϵ was calculated by using the scherrer's relation [12]

$$\epsilon = \frac{\beta}{4 \tan(\theta_o)} \quad (2)$$

where β (FWHM) describes the structural broadening, which is the difference in integral X-ray peak profile width between the sample and a standard (silicon) and is given by

$$\beta = \sqrt{\beta_{obs}^2 - \beta_{std}^2} \quad (3)$$

Assuming that the particle size and strain contributions to line broadening are independent to each other and both have a Cauchy-like profile, the observed line breadth is simply the sum of Equations (1) and (2), we get

$$\beta(2\theta) \cos \theta_o = \frac{k'\lambda}{D_v} + 4e(\sin \theta_o) \quad (4)$$

Equation (4) is customarily referred to as the "Williamson-Hall method" [13-15].

Fig. 3 illustrates $\sin(\theta_o)$ along the x-axis and $\beta(2\theta) \cos(\theta_o)$ along the y-axis for unexposed and exposed for 5, 10 and 15 shots of $Zn_{0.9}Co_{0.1}O$ thin films. The value of the crystallite size, (D_v) and lattice strain, (e) from the slope and the ordinate intersection respectively.

This behavior may be attributed to the increase in lattice defects among the grain boundary,

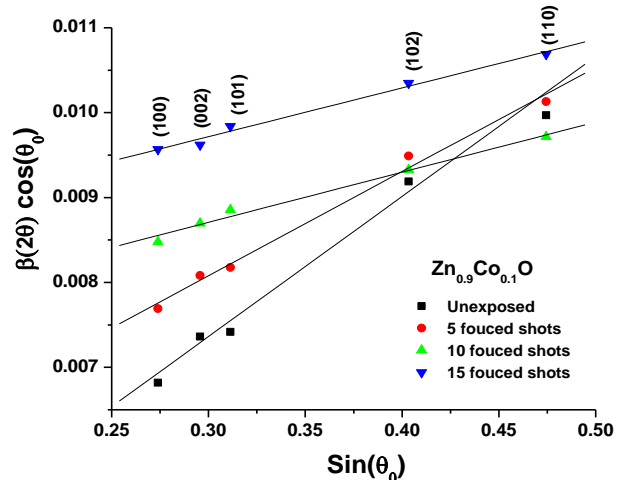


Fig. 3: linear fitting of $\beta(2\theta)\cos(\theta_0)$ versus $\sin(\theta_0)$ according to “Williamson Hall” method for calculating crystallite size and lattice strain.

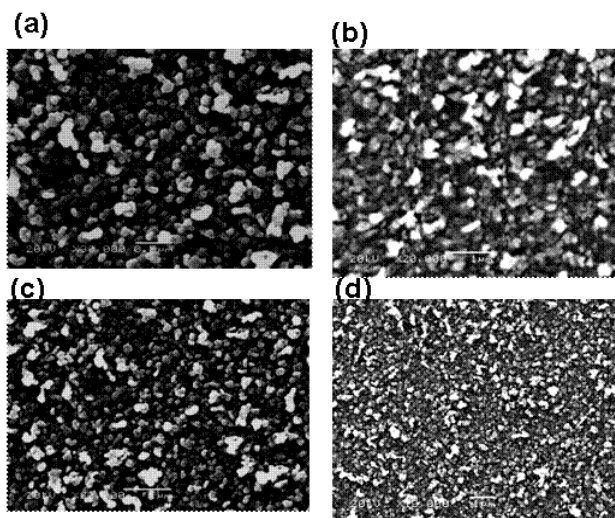


Fig. 4: SEM for of unexposed and exposed for 5, 10 and 15 plasma focusing shots of $\text{Zn}_{0.9}\text{Co}_{0.1}\text{O}$ thin films extended from (a) to (d), respectively.

Table 1: Microstructure parameters, optical band gap, E_g^{opt} , the single-oscillator energy E_o , dispersion energy E_d and refractive index $n(o)$ at $(E \rightarrow 0)$ for unexposed and exposed of plasma focusing shots of $\text{Zn}_{0.9}\text{Co}_{0.1}\text{O}$ thin films.

$\text{Zn}_{0.9}\text{Co}_{0.1}\text{O}$	D_v (nm) (XRD)	D_v (nm) (TEM)	e $\times 10^{-3}$	E_g^{opt} (eV)	E_d (eV)	E_o (eV)	$n(o)$
Unexposed	58.03	61±5	4.04	3.14	12.069	6.374	1.701
5 focused shots	35.07	39±4	3.08	2.86	12.092	5.691	1.808
10 focused shots	22.2	25±4	1.48	2.78	13.325	5.518	1.848
15 focused shots	19.26	18±3	1.438	2.67	13.568	5.42	1.872

where the grain size decreases. For more information on the crystal structure of our samples, the $\text{Zn}_{0.9}\text{Co}_{0.1}\text{O}$ thin film was analyzed by TEM. Fig. 4 (a-d) shows the morphology of the selected area electron diffraction (SAED) pattern of the unexposed and the exposed for 5, 10 and 15 shots of $\text{Zn}_{0.9}\text{Co}_{0.1}\text{O}$ thin films.

The SAED pattern shows no additional diffraction spots or rings of Co, CoO or Co_3O_4 phases, in good agreement with the XRD results. Fig. 4 (a-d) shows that the average size of grains decrease with increasing the PF shots. The estimated crystalline size using TEM is listed to table 1 and found to be in a good agreement with that those obtained from XRD peaks.

Table 1 shows a (D_v) and (e) of unexposed and exposed for 5, 10 and 15 shots of $\text{Zn}_{0.9}\text{Co}_{0.1}\text{O}$ thin films. It is observed that the (D_v) decreases with increasing the focusing in the restricted range (0, 5, 10, and 15 shots). The lattice strain (e) exhibited the same behavior i.e. decrease with increasing the focusing shots.

3.2 Optical properties

3.2.1 Determination of optical constants in terms of PF shots

The absolute values of the measured transmittance, $T(\lambda)$ and reflectance, $R(\lambda)$ were given according to the following equations [16, 17]

$$T = \left(\frac{I_{ft}}{I_g} \right) (1 - R_g) \quad (5)$$

where I_{ft} and I_g are the intensities of light passing through the film-glass substrate and the reference glass substrate, respectively.

$$R = \left(\frac{I_{fr}}{I_{Al}} \right) R_{Al} [1 + (1 - R_g)^2] - T^2 R_g \quad (6)$$

I_{fr} , I_{Al} are the intensities of light reflected from the sample and that from the reference mirror, respectively and R_g being the reflectance of glass. The variation of absolute value of $T(\lambda)$ and $R(\lambda)$ versus wavelength λ for the as deposited films of unexposed and exposed for 5, 10 and 15 shots of $Zn_{0.9}Co_{0.1}O$ thin films is shown in Fig. 5.

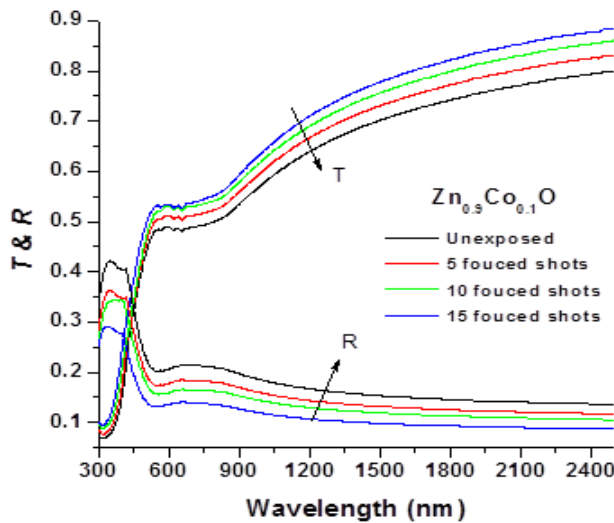


Fig. 5: Transmission and reflection versus wavelength for unexposed and exposed for 5, 10 and 15 shots of $Zn_{0.9}Co_{0.1}O$ thin films.

All the unexposed and exposed thin films show a sharp fall in transmittance at the fundamental absorption band edge. The sharp edge corresponds to electron excitation from the valance band to conduction band and interrelated to the nature and value of the optical band gap.

For determination the optical constants, refractive index n and extinction coefficient k , a method comprise a search technique based on minimizing $(\Delta T)^2$ and $(\Delta R)^2$ simultaneously has been used, where

$$(\Delta R)^2 = |R_{calc}(n, k, d, \lambda) - R_{exp}|^2 \quad (7)$$

$$(\Delta T)^2 = |T_{calc}(n, k, d, \lambda) - T_{exp}|^2 \quad (8)$$

where T_{exp} and R_{exp} are the experimentally determined values of T and R , respectively, and T_{calc} and R_{calc} are the calculated values of T and R , using Murmann's exact equation [18][19].

The adapted computation steps are as follows:

- 1- The measured transmittance, T_{exp} , measured reflectance R_{exp} , film thickness; d and the refractive index of substrate n_s are entered.

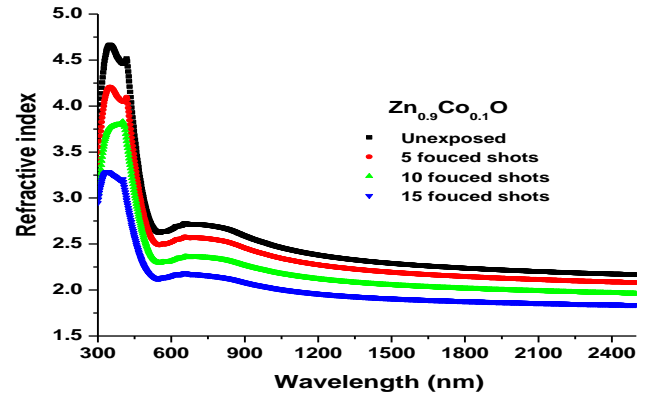


Fig. 6: Refractive index dispersion spectra of unexposed and exposed of plasma focusing shots of $Zn_{0.9}Co_{0.1}O$ thin films.

- 2- The film thickness d is an important parameter in the accurate determination of the optical constant. Therefore different methods have been used for determination of the thickness of the deposited films. Such thickness has been firstly estimated in situ by using a quartz crystal thickness monitor pre-calibrated interferometrically by using multiple beams Fizeau fringes at reflection [19].
- 3- Ranges of refractive index, n and ranges of the extinction coefficient, k within which the optimal solution is expected. The desired accuracy in n and k are putted as increments in n and k , respectively.
- 4- Using the Murmann's equation [18], both T_{calc} and R_{calc} are calculated throughout the whole ranges.
- 5- In each step the variances $(\Delta T)^2$ and $(\Delta R)^2$ are calculated and compared, to seek their simultaneous minimization. The corresponding values of n and k represent the solution. During the iteration, in some small regions of the spectrum the solutions may be missing. The missing part can be interpolated by using the program origin version 7 (OriginLab Corp.).

The optical constants, both the refractive index (n) and extinction coefficient (k) for unexposed and exposed for 5, 10 and 15 shots of $Zn_{0.9}Co_{0.1}O$ thin films is shown in Fig 7 and 8. It can be seen that the refractive index decreases with increasing the plasma focusing shots due to the reduction in the film thickness of the samples, which are clearly seen as an improvement in transmission spectra with increasing PF shots.

The spectral dependence data of the refractive index dispersion of the unexposed and exposed for 5, 10 and 15 shots of $Zn_{0.9}Co_{0.1}O$ thin films can be evaluated according

to the single-effective-oscillator model proposed by Wemple–DiDomenico (WDD) [20]. The model suggests that the refractive index, n , of the films could be correlated to the oscillator energy, E_o , and the dispersion energy, E_d , by the following formula:

$$n^2 = 1 + \frac{E_o E_d}{E_o^2 - (hv)^2} \quad (9)$$

Where (hv) is the photon energy and E_o , E_d is single-oscillator constants.

Fig. 8 shows the optical dispersion behavior, $(n^2-1)^{-1}$ versus $(hv)^2$, of the investigated thin films. The oscillator parameters E_o and E_d were determined by fitting a straight line to the points.

The slope of the linear relationship represents the $(E_o E_d)^{-1}$ and intercept with the vertical axis equal to (E_o/E_d) . The values obtained of dispersion parameters, E_o and E_d for unexposed and exposed for 5, 10 and 15 shots of $Zn_{0.9}Co_{0.1}O$ thin films are listed in Table 1. Furthermore, the oscillator energy E_o (or the effective oscillator energy) can be directly correlated with the optical energy gap E_g^{opt} by an empirical formula, $E_o = 2 \times E_g^{opt}$, as was found by

Tanaka [21]. It was observed that the values of E_g^{opt} are almost in agreement with that obtained from the Davis and Mott extrapolation model [22], see Table 1. Obviously, it is found that both E_o and E_d decrease with increasing PF shots. The decrease in the oscillator energy with composition may be attributed to the observed shift of the optical transmission spectra in the short wavelength region, which shifts the absorption edge towards lower energies.

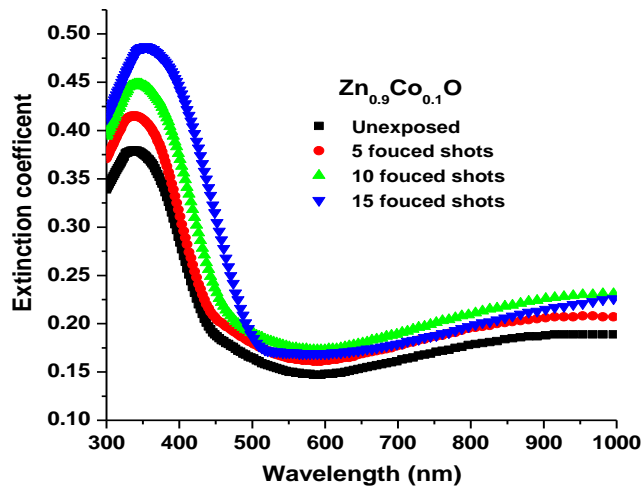


Fig. 7: The extinction coefficient versus wavelength of unexposed and exposed of plasma focusing shots of $Zn_{0.9}Co_{0.1}O$ thin films.

However, the decrease in the dispersion energy with PF shots can be understood as arising mainly from the changes

occurred in the film thickness of the samples with increasing PF shots.

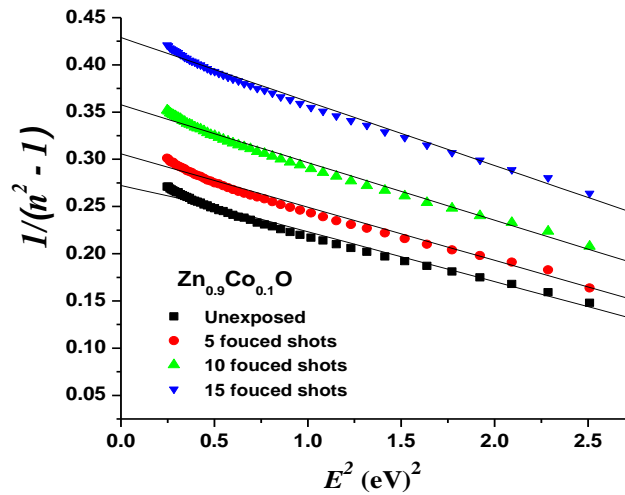


Fig. 8: Plot of refractive index factor $(n^2-1)^{-1}$ versus E^2 for unexposed and exposed of plasma focusing shots of $Zn_{0.9}Co_{0.1}O$ thin films.

Further analysis of the $(n^2-1)^{-1}$ against $(hv)^2$ allows to determine the static refractive index, using the following relation

$$n_o = (1 + E_d / E_o)^{0.5} \quad (10)$$

By extrapolating the WDD dispersion relation to the value of the incident photon energy hv approaching zero. The calculated values of the static refractive index n_o for all the investigated films are listed in Table 1. It was observed that the static refractive index decrease with increasing the PF shots due to the reduction of the film thickness.

3.2.2 Absorption coefficient and optical energy band gap in terms of PF shots

The absorption coefficient $a(hv)$ of unexposed and exposed for 5, 10 and 15 shots of $Zn_{0.9}Co_{0.1}O$ thin films can be calculated from the values of extinction coefficient k and λ using the known formula $k = a\lambda/4\pi$. Fig. 9 shows the absorption coefficient $a(hv)$ as a function of photon energy, hv for and exposed for 5, 10 and 15 shots of $Zn_{0.9}Co_{0.1}O$ thin films. It is known, that in the vicinity of the fundamental absorption edge, for allowed direct band-to-band transitions, the absorption coefficient is described by:

$$\alpha(hv) = \frac{K(hv - E_g^{opt})^m}{hv} \quad (11)$$

Where K is a characteristic parameter (independent of photon energy) for respective transitions, hv denotes photon energy, E_g^{opt} is optical energy gap and m is a number which characterizes the transition process. Many authors

[22-25] have suggested different values of m for different glasses, $m = 2$ for most amorphous semiconductors (indirect transition) and $m = 1/2$ for most of crystalline semiconductor (direct transition). In few reports, the band gap of unexposed and exposed samples are classified as a direct transition [26, 27] according to the polycrystalline nature of XRD samples, which are shown in Fig. 2. Therefore, the allowed direct optical band gaps of unexposed and exposed films were Evaluated from $(ahv)^2$ against hv plot. Fig. 10 shows $(ahv)^2$ vs. hv plots of different thickness of unexposed and exposed for 5, 10 and 15 shots of $Zn_{0.9}Co_{0.1}O$ thin films.

The $(ahv)^2$ versus hv plots of thin films exhibited a straight line and the intercept of energy axis at $(ahv)^2 = 0$ gives the direct energy band gap. The variation of direct band gap as a function of plasma focusing shots is listed in table 1. The values of direct E_g^{opt} are found to decrease with increasing the PF shots. The decrease of E_g^{opt} for direct transition may be attributing to the decrease in both the crystallites size and lattice strain. The optical band gap, E_g^{opt} decreases with increasing the PF shots because the crystal defects can be formed which produce localized states that change the effective Fermi level due to an increase in carrier concentrations [28-30] which attributed to the reduction in film thickness.

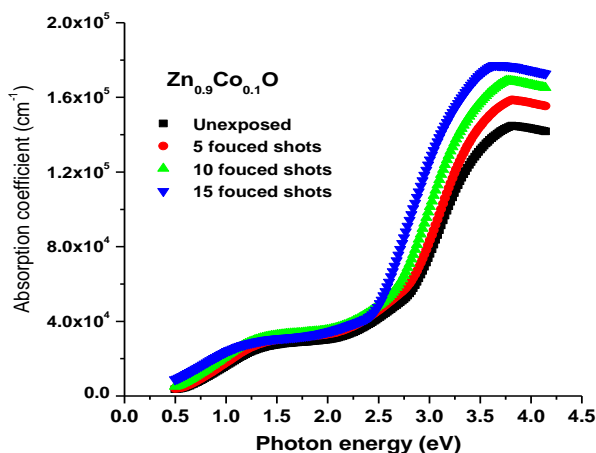


Fig. 9: The absorption coefficient $\alpha(hv)$ against photon energy hv of unexposed and exposed of plasma focusing shots of $Zn_{0.9}Co_{0.1}O$ thin films.

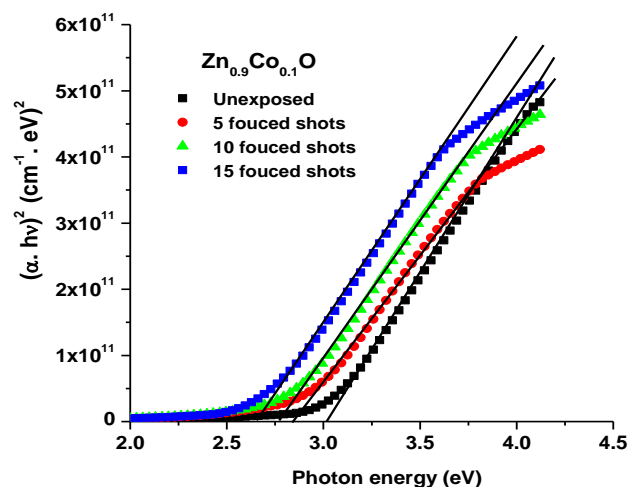


Fig. 10: The dependence of $(ahv)^2$ on photon energy hv of unexposed and exposed of plasma focusing shots of $Zn_{0.9}Co_{0.1}O$ thin films.

4 Conclusions

Nanoparticles of $Zn_{0.9}Co_{0.1}O$ were prepared by a homogeneous precipitation method. Thermogravimetric analysis (TGA) was used to identify the calcinations temperature for obtaining a high purity of $Zn_{0.9}Co_{0.1}O$ powder. Thin films with the same thickness of $Zn_{0.9}Co_{0.1}O$ were deposited by thermal evaporation of $Zn_{0.9}Co_{0.1}O$ from a modified source. The effect of plasma focusing shots (0, 5, 10 and 15 shots) on structural and optical properties of $Zn_{0.9}Co_{0.1}O$ thin films was studied. It is observed that the PF treatment can reduce both crystallite size and lattice strain of $Zn_{0.9}Co_{0.1}O$ thin films. The decreasing in lattice strain was attributed to the increase in lattice defects among the grain boundary, where the grain size decreases. For more information on the crystal structure of our samples, the $Zn_{0.9}Co_{0.1}O$ thin film was analyzed by TEM. The SAED patterns show no additional diffraction spots or rings of Co, CoO or Co_3O_4 phases, in good agreement with the XRD results. The estimated crystalline size using TEM was in a good agreement with that those obtained from XRD peaks. The optical properties were studied from their reflectance and transmittance in the spectral region in terms of the Murmann's equation. The refractive index has been found to decrease with increasing PF shots due to the reduction in film thickness. The dispersion of the refractive index is investigated using the WDD single oscillator model. The oscillator parameters were calculated. The optical energy gap has been estimated. The optical energy gap has been found to decrease with PF shots, which is explained on the basis of the decreasing both the crystallites size and lattice strain.

References

- [1] S. Lee, P Lee, G Zhang, X Feng, VA Gribkov, M Liu, et al. *IEEE Trans. Plasma Sci.* **26** (1998) 1119.
- [2] L. K. Lim, S. L. Yap and C. S. Wong, *AIP Conf. Proc.* **1328** (2011), p. 155.
- [3] C. M. Ng, S. P. Moo and C. S. Wong, *IEEE Transactions on plasma science* **26** (1998), p. 4.
- [4] C. B. Fitzgerald, M. Venkatesan, J. G. Lunney, L. S. Derneles and J. M. D. C. , *Applied Surface Science* **247** (2005), p. 493.
- [5] B. B. Nayak, B. S. Acharya, S. R. Mohanty, T. K. Borthakur and H. Bhuyan, *Surf. Coat. Technol.* **145** (2001).
- [6] C. R. Kant, M. P. Srivastava and R. S. Rawat, *Phys. Lett. A* **239** (1998), p. 109.
- [7] R. S. Rawat, P. Lee, T. White, L. Ying and S. Lee, *Surf. Coat. Technol.* **138** (2001), p. 159.
- [8] R. S. Rawat, W. M. Chew, P. Lee, T. White and S. Lee, *Surf. Coat. Technol.* **173** (2003), p. 276.
- [9] R. Gupta and M. P. Srivastava, *Plasma Sources Sci. Technol.* **13** (2004), p. 371.
- [10] S. Nunomura, K. Koga, M. Shiratani, Y. Watanabe, Y. Morisada, N. Matsuki and S. Ikeda, *Jpn. J. Appl. Phys. Part 2* **44** (2005), p. L1509.
- [11] J. Feugeas, G. Sanchez, C. O. de Gonzalez, J. D. Hermida and G. Scordia, *Rad. Eff. Defects in Solids* **128** (1994), p. 267.
- [12] B. D. Cullity, *Elements of X-ray diffraction. 2nd ed. London: Addison-Weasley; 1978.*
- [13] D.G. Morris, M. A. Morris and M. L. , *Materials Science and Engineering A* **156** (1992), p. 11.
- [14] G. H. Chen, C. Suryanarayana and F. H. Froes, *Metallurgical and Materials Transactions* **26A** (1995), p. 1379.
- [15] E. Szewczak, J. Paszula, A. V. Leonov and H. Matyja, *Materials Science and Engineering A* **226-228** (1997), p. 115.
- [16] L. A. Agiev and I. N. Shklyarevskii, *J. Prekel Spekt.* **76** (1978), p. 380.
- [17] N. El-Kabnay, E. R. Shaaban, N. Afify and A. M. Abou-sehly, *Physica B* **403** (2008), p. 31.
- [18] O.S. Heavens, *Optical Properties of Thin Films, Dover, New York, 1965.*
- [19] S. Tolansky, *Multiple-Beam Interference Microscopy of Metals, vol. 55, Academic Press, London, 1970.*
- [20] S. H. Wemple and D. , *Phys. Rev. B* **3** (1971), p. 1338.
- [21] T. Tanaka. , *Thin Solid Films* **66** (1980), p. 271.
- [22] E.A. Davis and N. F. Mott, *Philos. Mag.* **22** (1970), p. 903.
- [23] E. R. Shaaban, Ishu Kansal and José M. F. Ferreira *Physica B: Condensed Matter* **404** (2009), p 3571.
- [24] E. R. Shaaban, *Philos. Mag.* **88** (2008), p. 781.
- [25] E. R. Shaaban, M. Abdel-Rahman, El Sayed Yousef, M. T. Dessouky and T. S. Films, **515** (2007), p. 3810.
- [26] P. Pramanik and S. Bhattachraya, *J. Electrochem. Soc.* **137** (1990), p. 3869.
- [27] R.H. Misho, W.A. Murad, G.H. Fatahalah, I.M. Abdul-Aziz and H.M. Al-doon, *Phys. Stat. Solidi (a)* **109** (1988), p. K101.
- [28] E. R. Shaaban, *Appl. Phys. A* **115** (2014), p. 919.
- [29] E. Márquez, J.M. González-Leal, A.M. Bernal-Oliva, R. Jiménez-Garay and T. Wagner, *J. Non-Cryst. Solids* **354** (2008) 503.
- [30] E. R. Shaaban, *J. Alloys Compd* **563** (2013), p. 274.